PALAIOS
Emphasizing the impact of life on Earth's history

PALAIOS, 2010, v. 25, p. 183–195
Research Article
DOI: 10.2110/palo.2009.p09-084r

USING LASER ABLATION-INDUCTIVELY COUPLED PLASMA-MASS SPECTROMETRY (LA-ICP-MS) TO EXPLORE GEOCHEMICAL TAPHONOMY OF VERTEBRATE FOSSILS IN THE UPPER CRETACEOUS TWO MEDICINE AND JUDITH RIVER FORMATIONS OF MONTANA

RAYMOND R. ROGERS,[1]* HENRY C. FRICKE,[2] VITTORIO ADDONA,[3] ROBIN R. CANAVAN,[1] CHRISTOPHER N. DWYER,[1] CARA L. HARWOOD,[1] ALAN E. KOENIG,[4] RACHEL MURRAY,[1] JEFFREY T. THOLE,[1] and JOSEPHINE WILLIAMS[1]

[1]*Geology Department, Macalester College, Saint Paul, Minnesota 55105, USA;* [2]*Department of Geology, Colorado College, Colorado Springs, Colorado 80903, USA;* [3]*Department of Mathematics, Statistics, and Computer Science, Macalester College, Saint Paul, Minnesota 55105, USA;* [4]*U.S. Geological Survey, Denver Federal Center, Denver, Colorado 80225, USA*

e-mail: rogers@macalester.edu

ABSTRACT

Laser ablation-inductively coupled plasma-mass spectrometry (LA-ICP-MS) was used to determine rare earth element (REE) content of 76 fossil bones collected from the Upper Cretaceous (Campanian) Two Medicine (TMF) and Judith River (JRF) Formations of Montana. REE content is distinctive at the formation scale, with TMF samples exhibiting generally higher overall REE content and greater variability in REE enrichment than JRF samples. Moreover, JRF bones exhibit relative enrichment in heavy REE, whereas TMF bones span heavy and light enrichment fields in roughly equal proportions. TMF bones are also characterized by more negative Ce anomalies and greater U enrichment than JRF bones, which is consistent with more oxidizing diagenetic conditions in the TMF. Bonebeds in both formations show general consistency in REE content, with no indication of spatial or temporal mixing within sites. Previous studies, however, suggest that the bonebeds in question are attritional assemblages that accumulated over considerable time spans. The absence of geochemical evidence for mixing is consistent with diagenesis transpiring in settings that remained chemically and hydrologically stable during recrystallization. Lithology-related patterns in REE content were also compared, and TMF bones recovered from fluvial sandstones show relative enrichment in heavy REE when compared with bones recovered from fine-grained floodplain deposits. In contrast, JRF bones, regardless of lithologic context (sandstone versus mudstone), exhibit similar patterns of REE uptake. This result is consistent with previous reconstructions that suggest that channel-hosted microfossil bonebeds of the JRF developed via the reworking of preexisting concentrations embedded in the interfluve. Geochemical data further indicate that reworked elements were potentially delivered to channels in a recrystallized condition, which is consistent with rapid adsorption of REE postmortem.

INTRODUCTION

Geochemical approaches to the study of vertebrate fossils can reveal novel and often otherwise unavailable insights into the paleobiology and paleoecology of extinct animals (e.g., MacFadden et al., 1999; Fricke and Rogers, 2000; Schweizer et al., 2007; Clementz et al., 2008; Fricke et al., 2009). Geochemical data sets can also be applied to taphonomic questions that relate to the burial history and diagenesis of vertebrate remains. Early efforts to characterize the chemical taphonomy of vertebrate fossils generally focused on the nature of the authigenic minerals filling primary voids and the alteration of bioapatite to more stable phases in the burial environment (e.g., Rogers, 1924; Toots, 1963; Brophy and Nash, 1968; Piepenbrink, 1989; Person et al., 1995; Hubert et al., 1996; Barker et al., 1997; Wings, 2004). In recent years the emphasis has shifted to the characterization of trace element content, and numerous studies have documented the uptake of the lanthanide series rare earth elements (REE) in vertebrate fossils (e.g., Wright et al., 1987; Trueman and Benton, 1997; Reynard et al., 1999; Trueman, 1999; Staron et al., 2001; Trueman et al., 2003, 2006; Metzger et al., 2004; Patrick et al., 2004; Martin et al., 2005; Labs-Hochstein and MacFadden, 2006; Suarez et al., 2007; Tütken et al., 2008; Koenig et al., 2009). These efforts have highlighted the potential for deciphering key aspects of taphonomic history using REE, and have advanced our understanding of the process of fossilization.

In this report, laser ablation-inductively coupled plasma-mass spectrometry (LA-ICP-MS), a technique rarely used to document the diagenesis of vertebrate skeletal tissues (Kohn, 2008; Trueman et al., 2008; Koenig et al., 2009), is used to characterize the REE content of fossil bones collected from seven microfossil bonebeds and a selection of other isolated fossil occurrences in the Upper Cretaceous (Campanian) Two Medicine (TMF) and Judith River (JRF) Formations of Montana (Fig. 1). These two units are perfectly suited for a comparative study of geochemical taphonomy because both are richly fossiliferous, both can be studied in an existing stratigraphic framework (Rogers, 1998), and both preserve vertebrate fossils in a variety of paleoenvironmental contexts ranging from the alluvial uplands (TMF) to coastal plain lowlands (JRF) (Rogers and Kidwell, 2000). Moreover, the taphonomic histories of the copious fossils under investigation are well understood (Rogers, 1990, 1993, 1995; Rogers and Brady, 2010) and, thus, geochemical data can be evaluated in the context of independently derived taphonomic data sets that have already revealed formation-scale patterns and distinctions in the preservation of vertebrate remains.

Geochemical characteristics of fossil bones recovered from the TMF and JRF are first compared on the formation scale, and regional patterns in REE content that relate to paleoenvironmental controls on the uptake of trace elements are revealed. Geochemical characteristics of vertebrate elements are also characterized on a site-by-site basis within each formation, and facies-specific patterns of REE uptake are resolved. REE patterns based on LA-ICP-MS analyses are further used to test existing taphonomic reconstructions that relate to the origins of microfossil bonebeds in continental records (Rogers and Brady, 2010). This, in turn, offers novel insights into the diagenetic pathways that vertebrate hardparts follow to recrystallization and long-term preservation in alluvial successions.

STUDY AREA AND SAMPLE

TMF–JRF Interval

Fossils analyzed for REE content were recovered from proximal (upland) and distal (coastal) portions of a single eastward-thinning

* Corresponding author.

 0883-1351/10/0025-0183/$3.00

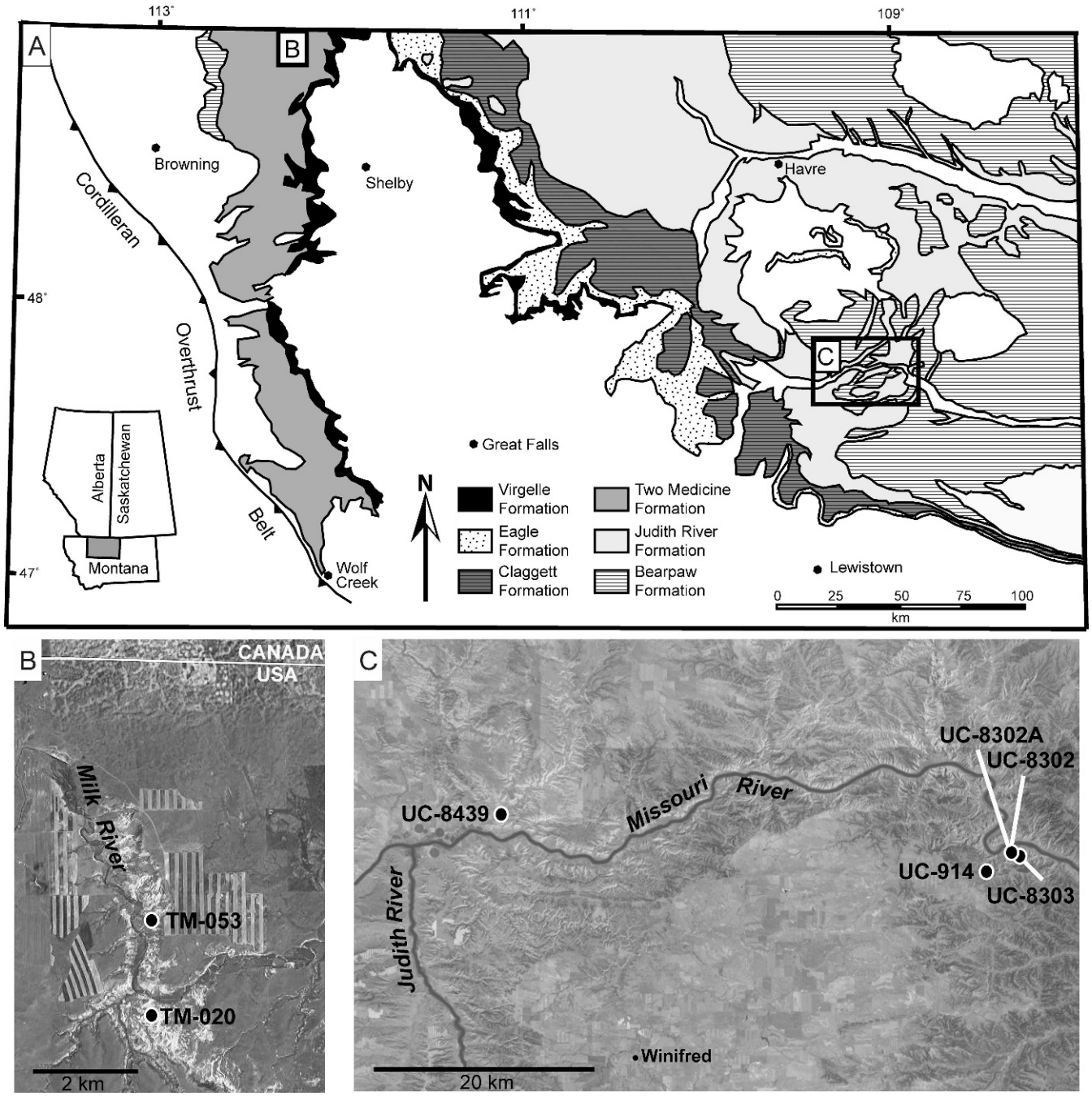

FIGURE 1—Field areas. A) Map of Upper Cretaceous units in northwestern and north-central Montana showing locations of Two Medicine Formation (Inset B) and Judith River Formation (Inset C) study areas. B) The Landslide Butte field area (Rogers, 1990), a localized pocket of badlands that includes exposures of the uppermost Two Medicine Formation and overlying Bearpaw Formation. C) Part of the Upper Missouri River Breaks National Monument, a vast region of badland exposures that includes the type area of the Judith River Formation. Inset images modified from Google Earth.

clastic wedge that accumulated along the western margin of the Western Interior Basin during the Late Cretaceous. Rocks in the up-dip portion of the study interval are included within the TMF, which crops out to the east of the Cordilleran fold and thrust belt in northwestern Montana (Fig. 1). In its type area along the Two Medicine River, the ~550 m thick TMF is characterized by fine- to medium-grained sandstones of predominantly fluvial origin intercalated with mudstones and siltstones that accumulated in interchannel settings (Rogers, 1995, 1998). TMF sites sampled for this study crop out near the top of the formation in the Landslide Butte field area (Rogers, 1990, fig. 1), and are associated with fluvial and shallow lacustrine deposits that accumulated in the alluvial uplands. Upland is used herein as indicative of being hundreds of kilometers distant from coeval shorelines of the Cretaceous Interior Seaway (Rogers, 1990, 1994, 1998). Previous studies indicate that in general the TMF was deposited under seasonal and semiarid conditions with sporadic rainfall (Rogers, 1990; Falcon-Lang, 2003). Radioisotopic age data (Rogers et al., 1993; Foreman et al., 2008) indicate that the TMF accumulated during the Campanian (83.5–70.6 Ma, Ogg et al., 2008), with deposition commencing prior to 80 Ma and ending shortly after 74 Ma.

Rocks in the more distal (coastal) portion of the study interval crop out in north-central Montana and are included within the JRF. In its

TABLE 1—REE concentrations (ppm) in fossil bones and associated sediments from the Two Medicine Formation.

Sample	La	Ce	Pr	Nd	Sm	Eu	Gd	Tb	Dy	Ho	Er	Tm	Yb
TM-020 1.1	3260.4	2681.2	608.4	2615.4	601.4	136.1	764.9	121.1	760.8	152.0	412.2	50.3	265.0
TM-020 1.2	2623.5	3045.9	763.7	3380.1	868.7	202.7	1008.0	163.2	974.1	180.9	458.9	53.2	253.6
TM-020 1.3	2627.3	2970.6	794.2	3742.7	1062.0	228.1	1211.5	197.8	1159.2	208.8	517.3	59.1	272.1
TM-020 1.4	750.2	911.9	112.7	512.1	124.3	40.9	219.9	39.6	308.5	77.7	256.7	37.4	223.7
TM-020 2.1	2168.2	2633.2	456.0	1989.7	482.1	115.8	597.7	94.5	588.3	115.3	308.2	37.2	182.6
TM-020 2.2	2272.9	2327.3	554.8	2407.0	609.2	141.6	760.4	123.5	766.5	148.3	393.5	47.2	230.0
TM-020 3.1	2531.2	2886.3	712.9	3213.6	793.8	189.9	917.5	144.4	862.7	159.7	398.6	46.6	222.0
TM-020 3.2	2071.6	2786.3	643.9	2750.5	676.1	143.6	782.1	123.5	737.7	139.1	355.4	42.6	209.0
TM-020 sed	31.7	63.1	7.7	29.3	6.1	1.2	5.1	0.8	4.9	1.0	2.7	0.4	2.5
TM-053 1.1	772.8	913.6	254.2	1212.1	309.7	83.8	455.2	75.1	460.0	93.3	226.1	26.6	119.1
TM-053 2.1	554.1	641.2	135.7	614.6	146.1	35.4	198.5	31.6	193.5	42.3	115.6	15.7	78.8
TM-053 3.1	649.3	1069.8	222.4	1078.5	300.6	72.6	412.8	68.4	430.7	85.6	220.3	25.4	119.2
TM-053 4.1	2213.6	2253.6	606.7	2543.3	539.9	128.2	583.7	89.3	499.6	93.7	216.1	23.6	98.7
TM-053 4.3	2573.5	2199.8	489.9	1923.0	396.1	88.0	411.9	64.7	381.3	76.1	193.3	23.9	114.0
TM-053 4.4	4104.7	3843.5	1632.9	8056.1	2312.5	490.2	2370.7	385.9	2061.5	355.2	787.1	89.4	381.3
TM-053 4.5	2575.2	2805.7	830.6	3762.3	944.8	197.7	885.7	142.1	782.7	137.5	318.4	36.5	164.6
TM-053 5.1	1596.1	1583.4	376.1	1800.2	465.2	121.5	606.6	99.3	612.1	124.5	316.3	39.9	187.7
TM-053 6.1	1254.0	1617.0	290.7	1169.3	303.4	36.5	344.2	59.5	359.5	67.7	171.4	21.4	105.3
TM-053 6.2	568.5	623.5	98.3	398.5	89.0	21.5	108.9	17.4	117.3	25.3	75.5	10.4	58.9
TM-053 6.3	2831.2	3789.2	1128.6	5172.7	1226.5	296.9	1325.2	201.4	1082.1	193.4	423.7	45.6	197.2
TM-053 6.4	2249.2	2528.4	638.0	2790.9	689.2	152.3	731.8	118.7	693.9	129.6	322.8	37.6	177.3
TM-053 6.5	1503.7	2076.0	281.9	1125.5	242.3	56.2	258.6	39.3	238.4	46.3	124.4	15.9	85.2
TM-053 sed	35.7	66.3	7.8	28.9	5.7	1.2	5.2	0.8	4.9	1.0	2.7	0.4	2.4
TMSS 2.1	363.5	532.8	92.6	508.1	164.9	44.2	299.1	58.4	441.2	105.6	326.6	44.4	232.2
TMSS 3.1	332.8	510.0	82.1	418.6	125.6	30.3	180.3	31.1	217.5	49.5	152.5	21.2	118.0
TMSS 4.1.1	675.0	784.8	107.1	442.4	104.8	23.2	151.1	26.7	191.9	45.7	148.0	22.0	125.1
TMSS 4.1.2	686.2	728.7	129.3	569.8	135.4	31.5	190.1	29.6	191.0	40.4	111.2	13.2	63.6
TMSS 4.2.1	45.7	40.7	3.8	14.9	3.4	0.9	9.9	1.1	9.0	2.7	10.2	1.7	10.8
TMSS 4.2.2	302.5	389.9	50.0	211.3	45.9	10.0	61.1	9.3	58.6	12.6	36.8	4.9	26.6
TMSS 5.1	801.6	769.2	138.1	574.1	126.4	31.1	176.8	29.2	196.3	45.0	132.5	17.8	92.4
TMSS 5.2	560.7	541.8	59.3	209.9	39.5	9.9	57.4	9.5	71.6	18.0	59.4	8.6	45.8
TMSS 6.1	535.2	809.5	141.3	620.1	143.3	33.2	182.4	28.7	175.1	35.6	99.1	12.0	59.9
TMSS 6.2	178.0	221.8	28.7	113.0	25.1	6.4	42.1	6.3	44.4	10.9	34.7	4.9	26.8
TMSS 5 sed	29.8	53.2	6.1	21.6	4.0	0.9	3.3	0.5	3.2	0.7	1.8	0.3	1.7
TMSS 6 sed	30.1	54.8	6.6	24.7	4.9	1.1	4.3	0.7	4.3	0.9	2.4	0.3	2.1

type area along the Missouri River (Fig. 1), the JRF is up to ~180 m thick, and is characterized by carbonaceous claystones, siltstones, and fine- to medium-grained sandstones of fluvial, tidal, and shallow marine origin. Beds of fissile lignite and ironstone are common, especially in upper reaches of the unit. The JRF accumulated under considerably more mesic conditions than correlative facies of the TMF (Rogers, 1998). Radioisotopic age data from the JRF and correlative units, combined with biostratigraphic data from associated marine units, indicate that the JRF is Campanian in age, and accumulated from ca. 79 to 74 Ma (Goodwin and Deino, 1989; Rogers, 1995; Rogers and Swisher, 1996; Foreman et al., 2008). JRF sites sampled for this study crop out in the upper half of the formation above a stratigraphic discontinuity interpreted to correlate with the widespread addition of accommodation that coincided with the Bearpaw transgression in the marine portions of the basin (Rogers, 1998; Rogers and Kidwell, 2000). This discontinuity is a few meters beneath a bentonite bed dated at ca. 75.5 Ma (Rogers and Swisher, 1996; R. Rogers and A. Deino, unpublished data, 2004).

Sampled Sites

Most fossils were recovered from microfossil bonebeds (Eberth et al., 2007; Rogers and Kidwell, 2007), which are localized concentrations of predominantly small (≥75% of elements ≤5 cm maximum dimension) disarticulated and dissociated skeletal material (bones, teeth, scales, scutes, spines, bone pebbles). This includes a variety of skeletal elements and fragmentary remains from small animals, including frogs, salamanders, fish, and mammals, and small skeletal elements or fragments from larger animals, including turtles, crocodiles, and dinosaurs. The potential origins of microfossil bonebeds have until recently remained an under-explored topic, with most previous considerations invoking some degree of transport in surface flows prior to final accumulation. In a recent study focusing specifically on the genesis of microfossil bonebeds, Rogers and Brady (2010) presented evidence that suggests that microfossil bonebeds can form *in situ* in low energy aquatic settings via attritional processes, and once concentrated, can be readily reworked by active channels and redeposited in close proximity to source beds. The current study offers an opportunity to test these taphonomic reconstructions using geochemical properties of fossils recovered from microfossil bonebeds and associated facies.

Two microfossil bonebeds were sampled in the TMF Landslide Butte field area (Fig. 1, Table 1). Both bonebeds (TM-020 and TM-053) are hosted by fine-grained facies that accumulated in shallow lakes populated by freshwater bivalves and gastropods (Rogers, 1990, 1995). In addition, isolated fossil bones were collected from five discrete fluvial sandstones stratigraphically associated with the TMF microfossil bonebeds.

Five microfossil bonebeds were sampled in the Missouri Breaks field area of the JRF (Fig. 1, Table 2). Three of the JRF bonebed localities (UC-8302A, UC-8303, UC-914) are preserved in fine-grained facies indicative of low energy aqueous depositional settings, such as floodplain ponds or lakes. All three preserve shell debris of freshwater invertebrates, including the bivalve *Sphaerium*, the gastropods *Viviparus*, *Campeloma, Lioplacodes*, and, more rarely, the aragonitic remains of the bivalve "*Unio*" (J. Hartman, personal communication, 2007). Two of the JRF microfossil bonebeds (UC-8302, UC-8439) are

TABLE 2—REE concentrations (ppm) in fossil bones and associated sediments from the Judith River Formation.

Sample	La	Ce	Pr	Nd	Sm	Eu	Gd	Tb	Dy	Ho	Er	Tm	Yb
UC-8302 2-1	217.5	545.7	76.8	291.1	51.6	20.9	58.5	14.0	47.5	14.0	39.6	5.3	28.1
UC-8302 2-2	161.7	329.0	50.0	209.4	42.7	18.1	61.1	14.8	57.6	16.4	52.9	7.0	37.6
UC-8302 2-3	879.8	1709.5	232.0	865.1	140.9	54.5	188	33.8	185.4	42.2	196.4	26.3	141.2
UC-8302 3-1	166.1	361.7	49.4	196.0	41.9	17.7	57.9	13.5	45.0	13.7	37.9	5.1	27.8
UC-8302 3-2	96.6	229.9	28.6	98.6	22.9	11.7	30.4	11.0	32.0	11.7	30.5	4.4	26.1
UC-8302 3-3	175.3	432.1	61.0	233.0	42.4	18.0	49.0	12.5	38.8	12.4	30.7	4.1	21.4
UC-8302 4-1	502.1	1118.7	151.8	551.3	95.2	35.5	121.9	23.5	110.9	26.9	110.4	15.4	85.3
UC-8302 4-2	184.3	445.7	64.7	253.8	42.5	18.7	49.7	12.5	38.3	12.3	30.1	4.0	21.1
UC-8302 4-4	252.6	578.3	82.2	314.8	59.6	23.0	70.0	15.5	56.8	15.6	47.0	6.1	32.7
UC-8302 sed	30.4	58.9	6.9	26.7	5.6	1.4	5.1	0.8	4.8	1.0	2.5	0.4	2.3
UC-8302A 1-1	168.2	419.8	57.7	220.1	45.7	17.7	60.6	14.9	56.6	16.2	52.1	7.2	40.1
UC-8302A 1-2	350.9	926.3	139.2	513.2	78.8	27.6	85.7	17.4	67.8	17.5	58.5	7.9	43.8
UC-8302A 1-3	980.7	2264.4	290.5	1039.6	78.6	66.3	228.9	38.5	204.9	44.2	197.8	26.0	138.4
UC-8302A 3-1	265.4	634.7	93.9	374.2	70.6	24.4	87.2	17.6	68.9	17.9	59.2	7.9	42.1
UC-8302A 3-2	143.9	340.9	49.0	192.2	38.7	15.8	53.7	12.7	39.3	12.5	31.7	4.2	22.4
UC-8302A 3-3	186.0	448.9	64.8	257.2	49.7	18.9	62.1	14.4	50.2	14.6	41.7	5.4	29.3
UC-8302A 3-4	175.1	418.5	59.7	239.2	46.3	18.1	58.7	14.0	48.1	14.1	39.0	5.0	27.1
UC-8302A sed	30.2	57.9	6.9	25.9	5.3	1.1	4.6	0.8	4.5	0.9	2.5	0.4	2.3
UC-8439 1-1	1404.8	3377.8	550.6	2072.1	317.3	105.0	386.4	64.6	375.9	75.2	345.1	43.3	212.9
UC-8439 1-2	1582.4	4452.1	671.3	2335.4	351.6	129.0	416.6	67.6	396.3	78.9	366.5	46.4	232.6
UC-8439 2-1	760.0	2019.2	323.7	1132.2	172.3	55.5	204.0	35.7	193.4	44.2	205.1	27.6	145.0
UC-8439 2-2	1315.6	3681.5	732.4	2177.5	318.1	102.2	350.9	57.6	323.0	65.3	297.2	37.3	187.7
UC-8439 2-3	1202.0	3315.9	604.8	1768.7	264.8	91.8	318.4	54.4	311.7	63.0	282.2	35.3	173.8
UC-8439 3-1	232.4	492.6	71.6	278.0	44.7	18.6	57.8	14.7	57.3	16.9	58.1	8.1	45.1
UC-8439 3-2	1093.1	3173.9	612.5	1769.1	254.0	83.0	285.2	48.0	269.0	57.0	265.3	34.6	179.0
UC-8439 3-3	1724.9	3988.7	698.7	2716.9	425.6	139.7	517.5	84.7	506.3	99.5	459.9	55.9	272.4
UC-8439 4-1	35.0	55.1	7.8	36.9	12.6	8.9	27.6	11.4	53.4	21.2	110.7	18.4	115.6
UC-8439 4-2	542.5	1135.4	179.5	759.1	129.8	55.3	218.2	45.1	318.3	77.4	408.9	55.3	285.8
UC-8439 4-3	236.7	422.0	65.0	264.5	45.7	21.3	72.7	18.8	101.1	29.2	141.4	20.5	118.0
UC-8439 sed	30.1	56.9	6.7	24.7	4.8	1.0	4.0	0.6	3.8	0.8	2.0	0.3	1.9
UC-914 1	262.7	450.9	75.8	337.3	90.8	22.1	113.4	18.0	114.2	24.0	70.6	10.1	55.9
UC-914 2	162.5	272.5	46.2	206.9	57.1	14.2	73.7	11.6	74.5	15.4	46.3	6.4	36.5
UC-914 3	587.2	876.6	168.6	783.9	223.9	56.7	307.8	49.5	315.6	64.5	186.6	25.2	137.2
UC-914 4	189.4	302.9	54.6	251.6	70.9	18.0	99.6	14.5	93.7	18.9	55.9	7.6	43.8
UC-914 5	811.4	1202.0	174.4	710.8	238.5	71.4	331.5	55.6	350.7	66.8	186.5	25.1	133.4
UC-914 6	180.8	271.9	42.1	177.2	51.6	14.9	68.3	9.4	57.0	10.7	29.5	4.0	21.6
UC-914 7	219.0	332.0	52.5	216.7	63.9	18.6	82.7	12.1	73.7	13.4	36.7	4.9	27.0
UC-914-8	2962.0	3080.3	798.0	3306.2	953.4	253.4	1041.3	165.2	963.1	175.4	457.6	57.7	293.1
UC-914 sed	40.6	76.5	9.2	35.3	7.3	1.6	6.8	1.1	6.5	1.3	3.6	0.5	3.1
UC-8303 1	795.0	1103.0	159.1	679.9	216.1	57.8	290.8	49.8	318.8	63.7	184.0	28.4	154.2
UC-8303 2	255.0	480.2	57.4	253.0	72.5	21.7	94.8	14.8	87.6	18.7	50.5	7.7	44.0
UC-8303 3	59.4	60.9	9.4	44.3	12.8	3.0	15.2	3.1	23.1	5.4	19.5	3.6	26.5
UC-8303 4	322.3	355.1	45.3	178.9	54.0	18.0	109.1	16.9	121.7	28.9	93.8	14.3	86.3
UC-8303 5	538.7	690.9	98.1	396.9	127.5	43.8	229.5	39.6	280.2	63.8	196.4	27.0	149.1
UC-8303 6	825.4	1190.6	179.2	738.1	204.4	54.9	267.4	43.4	280.6	58.3	171.4	24.4	141.3
UC-8303 7	1238.5	1755.4	268.8	1098.3	308.7	83.9	409.3	70.0	478.1	102.8	320.3	47.3	279.3
UC-8303 8	2689.8	2552.6	632.1	2511.1	640.6	163.2	732.5	116.7	736.4	149.0	434.0	58.3	326.3
UC-8303 9	2897.0	2984.9	790.3	3287.1	925.2	227.9	1068.7	170.2	1033.1	201.2	555.1	73.7	394.0
UC-8303 10	743.3	1033.6	139.9	536.4	185.2	53.9	277.8	45.9	292.6	60.0	176.8	25.0	138.5
UC-8303 sed	37.9	72.5	8.8	34.6	7.1	1.6	6.5	1.0	6.3	1.2	3.3	0.5	2.8

hosted by fluvial sandstones, with fossils concentrated along basal and internal surfaces in association with intraformational pebbles and carbonaceous debris.

RATIONALE AND PREVIOUS WORK

Bone consists of crystallites of carbonated calcium phosphate (bioapatite) deposited in an organic matrix of collagen, with collagen typically comprising 25%–35% by volume of bone tissue, discounting vascularity (Trueman, 2007; Trueman et al., 2008). With the postmortem hydrolysis of collagen, metastable crystallites of bioapatite are exposed to reactive pore fluids that generally encourage dissolution and recycling of both organic and biomineralized materials. If conditions are favorable and fossilization occurs, the stabilized Ca-phosphate crystallites typically exhibit larger crystallite size and elevated fluorine content consistent with alteration to fluorapatite (francolite). Moreover, fossilized bone mineral typically preserves significantly elevated concentrations of trace elements, including REE and U, relative to that found in living bone tissue.

Several recent studies describe how bone incorporates trace elements during recrystallization (e.g., Trueman, 1999, 2007; Trueman and Tuross, 2002; Kohn, 2008; Koenig et al., 2009) and, thus, only a brief overview is provided here. In a commonly invoked model of bone fossilization (Hubert et al., 1996; Kolodny et al., 1996; Trueman, 2007), authigenic apatite is added to preexisting biogenic crystallites until the inter-crystallite porosity generated by the removal of collagen is filled. During addition of authigenic apatite to bioapatite seed crystals (Hubert et al., 1996) trace elements, including the REE, are adsorped from pore waters onto growing crystallite surfaces (Reynard et al., 1999; Trueman and Tuross, 2002). The uptake of trace elements is encouraged by the fact that bone crystallites have relatively large surface areas and high cation exchange capacities, and the REE readily

substitute into cation sites in the apatite lattice (Trueman et al., 2008). Upon recrystallization exchange capacity is diminished, and REE signatures are essentially locked in and preserved through subsequent diagenetic processes. Recrystallization accompanied by incorporation of REE has been estimated to occur within 10^3–10^5 years postmortem (Trueman and Tuross, 2002; Patrick et al., 2004).

The final trace element composition of fossil bone reflects the overall concentration of trace elements in the burial environment, the chemistry of the burial environment, and the hydrology of the burial environment (e.g., well-drained versus waterlogged soils), among other factors (Trueman, 2007; Kohn, 2008). This, in turn, renders the fractionation of the REE predictable with regard to particular environmental settings, and several case studies have used this predictability to explore the geochemical taphonomy of various burial environments. For example, Trueman and Benton (1997) compared REE concentrations among fossil bones and associated sediments from the Triassic of England, and demonstrated that REE are sensitive indicators of the sedimentary environment of early diagenesis. This was used to argue that the vertebrate fossils preserved in the marine Aust Cliff bonebed were allochthonous and reworked in a prefossilized condition from preexisting deposits. Trueman (1999) and Suarez et al. (2007) examined patterns of REE uptake in various continental deposits of Cretaceous age, and applied REE data sets to questions of time averaging and the mixing of remains in vertebrate assemblages. Patrick et al. (2004) analyzed REE in mosasaur bones from the marine Pierre Formation (Upper Cretaceous) of South Dakota, and demonstrated that REE track lithologic units (in this case members of the Pierre Formation) over considerable distances. These authors further concluded that REE signatures in fossil bones were reliable indicators of redox conditions related to ocean circulation patterns on the Late Cretaceous seafloor. Along these same lines, Labs-Hochstein and MacFadden (2006) reconstructed paleoceanographic conditions using the REE content of Cenozoic shark centra, and found that the REE provided key insights into the mixing of marine and fresh waters in nearshore settings. Shifting back to fully continental deposits, Metzger et al. (2004) documented REE patterns in paleosol profiles in the Oligocene Brule Formation in an effort to track the effects of pedogenesis on REE composition. They found that variations in bone REE track pedogenic development, and that bones fossilized in paleosols could be distinguished from bones recovered from sediments unaffected by pedogenic processes.

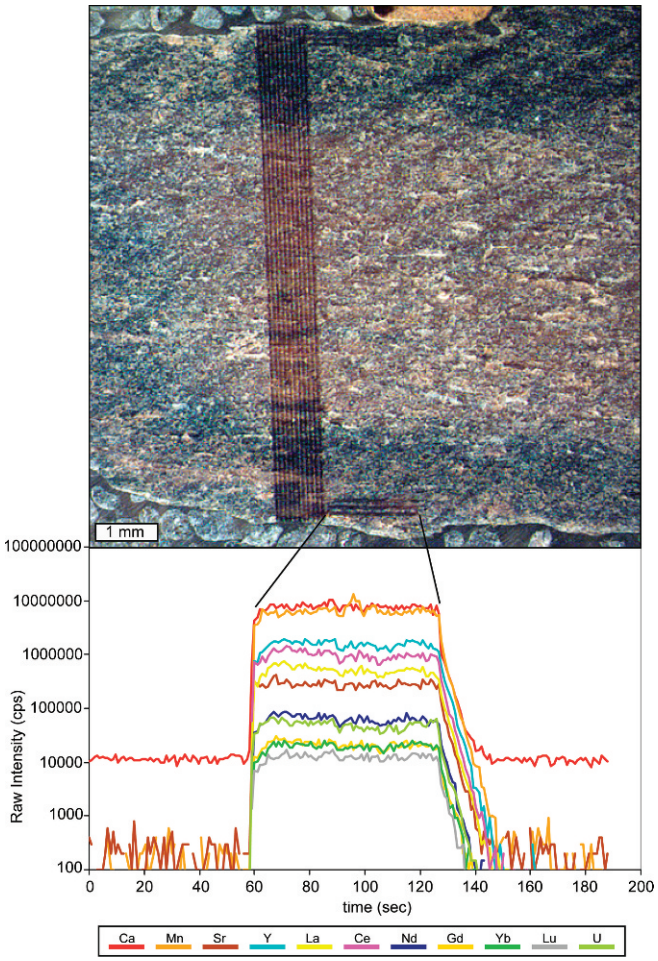

FIGURE 2—Laser ablation line scans on a bone from JRF bonebed UC-8303. Representative spectra from a single line scan (outermost line in basal set of three) shows raw intensity (counts per second) of selected elements (the number of elements graphed has been reduced for clarity). For each line scan all elements are collected simultaneously. The elongate set of vertical line scans is the LA-ICP-MS trace element map area from Koenig et al. (2009).

METHODS

LA-ICP-MS

Most previous studies of the REE in fossil bone have used conventional solution nebulization inductively coupled plasma-mass spectrometry (ICP-MS) to determine the composition of trace elements. Sampling for this technique typically involves the drilling of cortical bone and the dissolution of recovered powder in acids. Under ideal circumstances only bone tissue is sampled, and both mechanical and chemical techniques are used to avoid contamination by adhering detrital sediment and authigenic void-fill minerals. Analyses of the sampled powders are generally assumed to represent the average composition of the bone cortex (Trueman, 2007), although some workers (e.g., Tütken et al., 2008) have attempted to strategically drill and sample distinct fields of bone tissue (e.g., outermost cortex versus central compacta) in an effort to more precisely track the complexities of diagenesis.

Trace element compositions of fossil bone can also be characterized using laser ablation-inductively coupled plasma-mass spectrometry (LA-ICP-MS). LA-ICP-MS allows for the rapid analysis of large samples with minimal sample preparation, and permits the researcher to precisely target tissues (e.g., cortical bone, enamel, dentine) with exacting spatial resolution (see Durrant, 1999; Durrant and Ward, 2005; Grun et al., 2008; Koenig et al., 2009). LA-ICP-MS is regularly utilized in mineralogical studies and U–Pb geochronology, but has seen only limited application in the realm of paleontological research (e.g., Imai, 1992; Eggins et al., 2003; Rodland et al., 2003; Kohn, 2008; Grun et al., 2008). This is unfortunate, because LA-ICP-MS is arguably an ideal analytical tool to capture the trace-element composition of complex materials including fossil bones and teeth (Koenig et al., 2009).

Seventy-six bones were analyzed using LA-ICP-MS (Fig. 2). Bones were first set in epoxy blocks in order to prepare standard thin sections for petrographic and SEM analyses. After cutting and polishing, bone-bearing blocks were placed directly in the sample chamber of the LA-ICP-MS system. A CETAC Technologies LSX-500 laser ablation system operating at 266 nm was used for analyses. Ablated aerosol was introduced to the PerkinElmer ELAN6000 quadrupole ICP-MS. The operating conditions of the LA and ICP-MS systems are presented in Table 3. A prototype USGS Ca-phosphate reference material was used for calibration and quantification. This reference material is a close matrix match to bioapatite. Calcium at an average bioapatite concentration of 37 wt% was used as the internal standard element and quantification was done using standard concentration equations of Longerich et al. (1996). Quantification of Lu using the Ca-phosphate reference material was not possible because Lu was not in the reference

TABLE 3—Summary of LA-ICP-MS operating conditions. Detection limits for the REE range from 0.1 to 0.5 ppm.

Laser ablation system: LSX-500 (266 nm)	
Spot size	100 μm
Pulse frequency	5 Hz
Energy density	~15 J/cm^2
Scan speed	75 μm/sec
ICP-MS: Elan6000	
rF Power	1400 W
Carrier gas flow (He)	0.8–0.9 l/min
Makeup gas (Ar)	0.62 l/min

material. Detection limits for the entire data set are generally 0.1 to 0.5 ppm for REE.

Line scans were visually targeted to avoid large primary voids (e.g., vascular canals), fractures, and authigenic inclusions. Samples were analyzed using 2–3 continuous line scans per bone. Scans were typically targeted along the outer edges of bones (Fig. 2). Visual inspection of time resolved ICP-MS spectra (Fig. 2) often revealed variations in REE content related to zoning, fractures, and secondary inclusions. Scans were integrated in regions where spectra exhibited stable plateaus. All REE data presented in Tables 1–2 are mean concentrations for individual bones based on multiple individual line scans. Concentrations were normalized to the North American Shale Composite (NASC) using values reported in Gromet et al. (1984) and Haskin et al. (1968, for Pr, Ho, and Tm).

Additional Analyses

The REE content of sediments yielding fossil bones was determined by ICP-MS at Washington State University GeoAnalytical Lab. A Sciex Elan model 250 ICP-MS was used for analyses. Lu content is not reported for sediment samples because values for fossil bone are not available for comparison. Fourier Transform Infrared Spectroscopy (FT-IR) was used to further characterize the recrystallization of bioapatite. Samples were analyzed on a Nicolet Magna 550 infrared spectrometer at Macalester College. Spectra were examined to determine fluorine content and the relative abundance of carbonate and phosphate ions using methods outlined in MacFadden et al. (2004), Sponheimer and Lee-Thorp (1999), Weiner and Bar-Yosef (1990), and Shemesh (1990). Thin sections of bones were analyzed using SEM and standard petrographic techniques to document authigenic minerals and detrital materials in bone voids (fractures, vascular canals, etc.).

RESULTS

Bone Mineralogy

Bioapatite samples from TMF and JRF bones yield FT-IR spectra consistent with the presence of fluorine, with a peak positioned at 1096 cm^{-1}. This confirms that the fossil bones under investigation have recrystallized to francolite (carbonate fluorapatite), as is typical of fossilized bone (Elorza et al., 1999). In addition, fossil bones from the TMF and JRF are invested with a variety of authigenic minerals, including carbonates (calcite, ankerite), sulfides (pyrite), sulfates (barite, celestine), iron oxides (hematite), chlorite, and authigenic phosphate. A report detailing the distribution of authigenic minerals and detrital fills in fossil bones of the TMF and JRF is forthcoming (R. Rogers, unpublished data, 2009).

Formation-Scale Comparisons of REE Content

REE concentrations in ppm of the 76 bones analyzed in this report are compiled in Tables 1–2, as are REE concentrations of the sedimentary facies that yield fossil bones. Within the TMF, total per bone REE content ranges from 155 to 26871 ppm (mean = 7557 ppm, median = 5800 ppm, standard deviation = 6094 ppm). In the JRF, total per bone REE content ranges from 286 to 14608 ppm (mean = 4020 ppm, median = 1764 ppm, standard deviation = 3971 ppm). These values, which are in line with REE concentrations reported in previous studies (e.g., Trueman et al., 2006; Suarez et al., 2007), indicate that in general fossil bones in the TMF are characterized by higher REE content, and more variability in REE enrichment, than fossil bones in the JRF. In all cases, fossil bones from the TMF and JRF are characterized by higher REE content than the sedimentary facies that yield them (see Tables 1–2). Within the TMF, total REE content of facies that yield fossil bones ranges from 127 to 163 ppm (mean = 146 ppm, median = 147 ppm, standard deviation = 16.8 ppm). In the JRF, total REE content of facies that yield fossil bones ranges from 138 to 194 ppm (mean = 161 ppm, median = 147 ppm, standard deviation = 25.9 ppm).

Distinctive patterns in the distribution of light, middle, and heavy REE are evident between formations when comparisons are made using shale-normalized values. For example, the ratio of shale-normalized concentrations of La and Yb serves to readily distinguish the TMF from the JRF (Fig. 3). All but one fossil bone in the JRF sample is relatively enriched in heavy REE. In contrast, bones analyzed from the TMF show a greater range in La_n/Yb_n values spanning heavy and light enrichment fields in roughly equal proportions. The significance of this pattern in the distribution of REE was assessed using empirical cumulative distribution functions (ecdfs) of La_n/Yb_n for both the TMF and JRF. The two distributions (Fig. 3B) were found to be distinct ($p = 2.6 \times 10^{-8}$) using the nonparametric Kolmogorov-Smirnov test. The Kolmogorov-Smirnov test quantifies the distance between the two ecdfs, and is advantageous because it (1) necessitates no assumption about the distribution of the data (in particular no normality assumption is needed), and (2) is not only sensitive to differences in location, but to differences in spread and shape of the distributions as well.

Cerium (Ce) content also varies significantly among bones recovered from the TMF and JRF. Fossil bones from the TMF are characterized by more negative Ce anomalies than counterparts in the JRF record. Several TMF bones with negative Ce anomalies also exhibit relative enrichment in uranium, with U concentrations averaging 222 ppm in the TMF versus 49 ppm in the JRF (Fig. 4A). The distributions of the Ce anomaly in fossils from the TMF and JRF were found to be distinct with a p-value of 2.2×10^{-7} (Fig. 4B).

REE in Facies Context

REE content in fossil bones was also documented on a site-by-site basis. Spider diagrams of normalized REE data exhibit general consistency within localities (Fig. 5). The two pond-lake microfossil bonebeds sampled from the TMF (TM-053, TM-020) are characterized by pronounced negative cerium anomalies and relative enrichment of middle REE (e.g., Figs. 5A–B). Ten bones recovered from fluvial facies of the TMF show a pattern of relative enrichment in heavy REE (Fig. 5C). Four microfossil bonebeds sampled from the JRF (UC-914, UC-8302, UC-8302A, UC-8303) exhibit depletion of light REE and minor enrichment in middle and heavy REE (Figs. 5D–G). Bonebed UC-8439 from the JRF exhibits a nearly flat fractionation pattern relative to NASC (Fig. 5H).

REE content was further assessed in relation to preservation in sandstone and mudstone lithofacies (Figs. 6A–B). This distinction presumably tracks whether a bone underwent diagenesis in the sediments of a channel belt (sandstone) or in the finer-grained sediments characteristic of interchannel settings (mudstone). Bones recovered from the continental sandstones and mudstones of the TMF yield REE data that serve to distinguish fossils relative to facies context (Fig. 6A). For example, the ecdfs of Pr_n content in fossils from

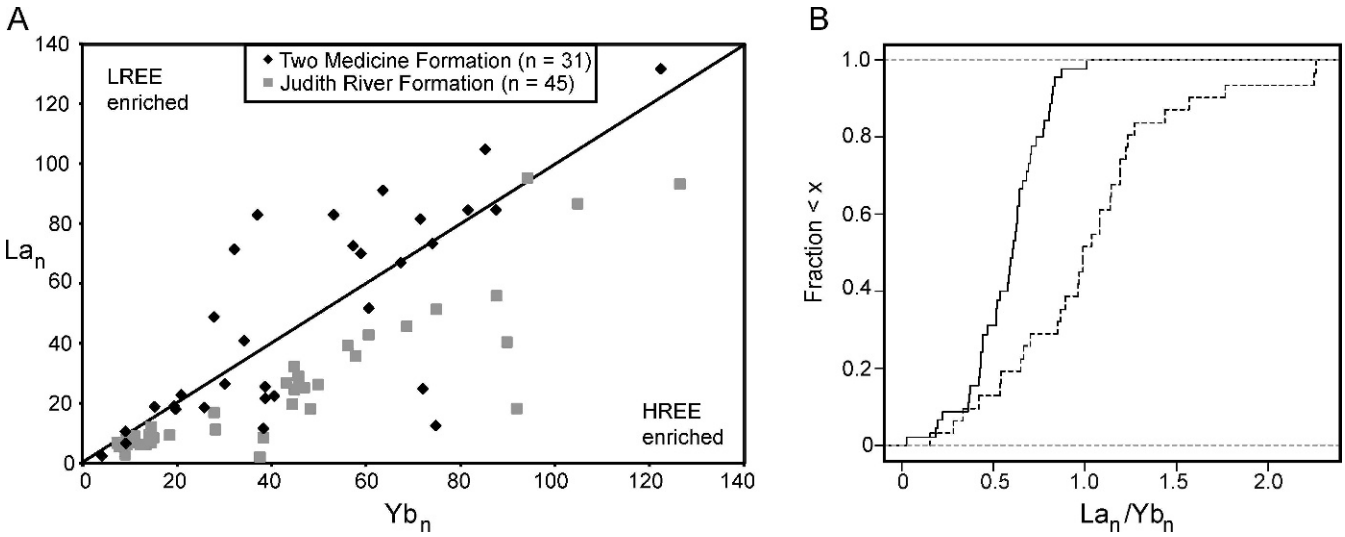

FIGURE 3—Shale-normalized concentrations of La and Yb readily distinguish the TMF from the JRF. A) Ratio of normalized La and Yb concentrations in fossil bones. All but one fossil bone in the JRF sample is relatively enriched in heavy REE. Bones from the TMF show a more variable pattern of enrichment. B) Empirical cumulative distribution functions (ecdfs) of La_n/Yb_n for the JRF (solid) and the TMF (dashed) were found to be distinct with a p-value of 2.6×10^{-8} (Kolmogorov-Smirnov test).

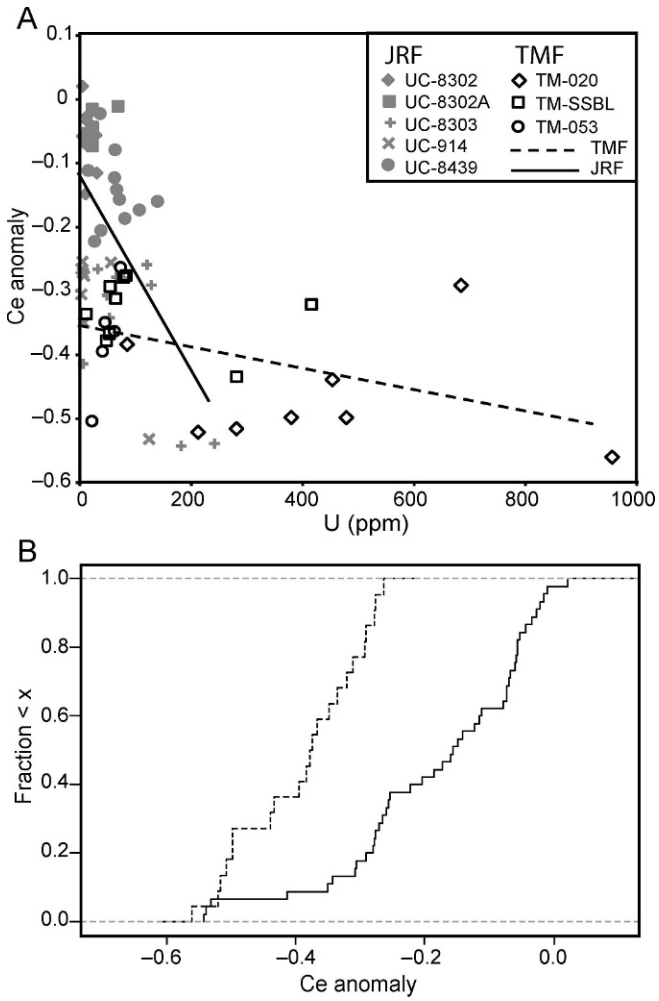

FIGURE 4—Cerium (Ce) content varies significantly in bones recovered from the TMF and JRF. A) Fossil bones from the TMF are characterized by more negative Ce anomalies than counterparts in the JRF record. Several TMF bones also exhibit relative enrichment in U. B) Distributions of the Ce anomaly in fossils from the TMF (dashed) and JRF (solid) are distinct with a p-value of 2.2×10^{-7} (Kolmogorov-Smirnov test).

sandstone and mudstone facies of the TMF were found to be distinct with a p-value of 2.1×10^{-5} (Fig. 6C). The difference between mudstone- and sandstone-derived fossils in the TMF held when modeling the ranks of Pr_n and controlling for Yb_n content ($p = 5.1 \times 10^{-5}$). In contrast, no significant distinctions were evident ($p = 0.4249$) when Pr_n content of fossil bone was compared among mudstone and sandstone sites of the JRF (Figs. 6B, D).

DISCUSSION

Comparisons with Previous Studies

The LA-ICP-MS approach utilized herein to determine REE content of fossil bones in the TMF and JRF yields results consistent with previous work in these same units (Trueman, 1999). Most notably, the shale-normalized pattern of La_n/Yb_n that serves to distinguish the TMF from the JRF in this study (Fig. 3) was also documented by Trueman (1999), albeit for a different pair of shale-normalized light (Pr) and heavy (Yb) REE; data from this study also yield statistically significant distinctions using Pr_n/Yb_n. In parallel with findings herein, Trueman (1999) found fossil bones from the Dinosaur Park Formation (DPF)—strata in Alberta equivalent to the JRF in Montana—to be predominantly HREE-enriched, and bones from the TMF to be more variable, spanning both heavy and light REE enrichment fields.

Trueman (1999) reported total REE contents ranging from 19 to 9300 ppm (mean 1136) for the TMF and 30 to 4600 ppm (mean 1544) for the DPF, and reasoned that these concentrations were somewhat lower than expected given the volcaniclastic nature of the host formations (e.g., Samilov and Benjamini, 1996). LA-ICP-MS analyses yielded total REE contents ranging from 155 to 26870 ppm (mean 7123) for the TMF and 286 to 14608 ppm (mean 4010) for the JRF. The higher concentrations reported herein are more in line with the well-documented volcaniclastic composition of the TMF and JRF (Lorenz, 1981; Rogers, 1990, 1998; Rogers et al., 1993; Foreman et al., 2008). Moreover, they vary as expected (TMF > JRF) given the proximity of the TMF to volcanic source areas. Reasons for discrepancies in REE concentration between this study and Trueman's (1999) are unknown, but probably imply some combination of different sampling strategies—precise targeting of outermost cortical tissue using LA-ICP-MS versus drilling of bone cortex—and different sedimentological context. Bones utilized in this study were collected higher in section within the

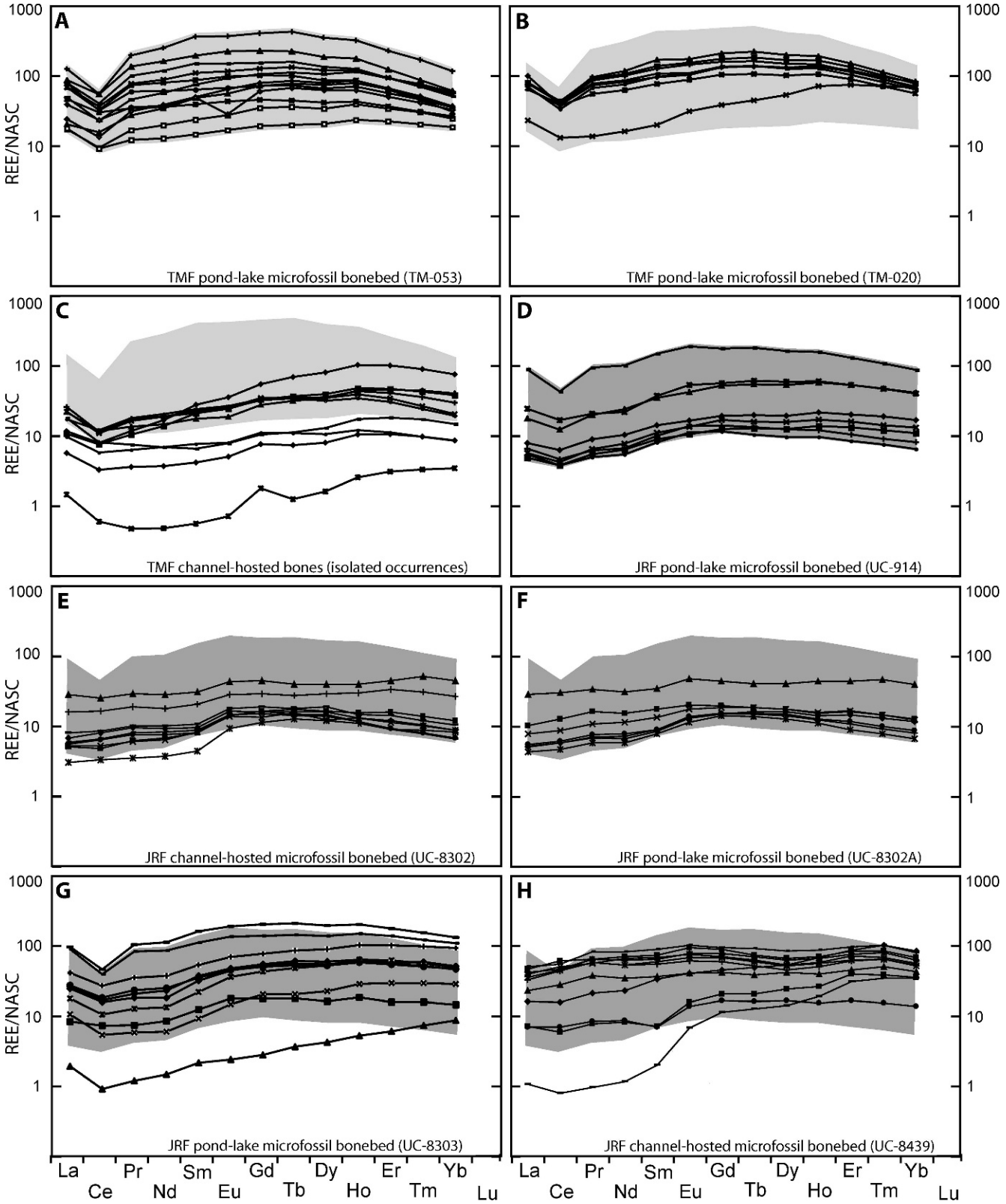

FIGURE 5—Shale-normalized REE patterns exhibit general consistency within localities. A,B) Pond-lake microfossil bonebeds of the TMF (TM-053, TM-020) characterized by pronounced negative Ce anomalies and relative enrichment of middle REE. C) The ten bones recovered from fluvial sandstone bodies of the TMF show relative enrichment in heavy REE. Light gray field in A–C represents the REE signature of TM-053. Bones recovered from sandstone facies in C show a pattern of fractionation distinct from the TM-053 REE field. D–G) Four of the microfossil bonebeds sampled in the JRF (UC-914, UC-8302, UC-8302A, UC-8303) exhibit depletion of light REE and minor enrichment in middle and heavy REE. H) Bonebed UC-8439 from the JRF exhibits a flatter fractionation pattern relative to NASC, but still shows minor enrichment in middle and heavy REE; dark gray field in D–H represents the REE signature of UC-914. All bones recovered from the JRF essentially conform to this pattern, with rare exceptions (see text for discussion of outliers).

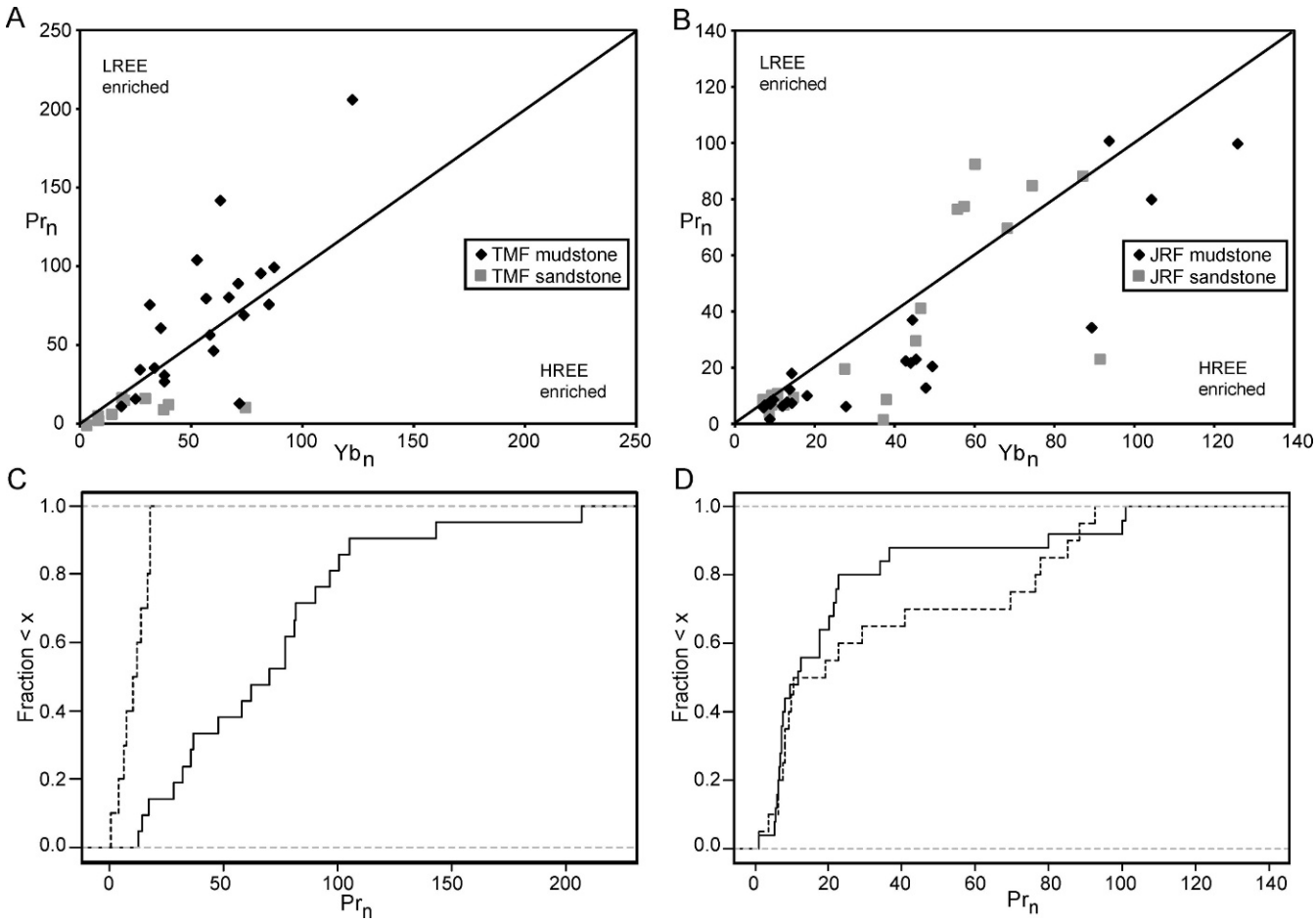

FIGURE 6—REE content was assessed in relation to preservation in sandstone and mudstone. A) Bones recovered from continental sandstones and mudstones of the TMF yield REE data that serve to distinguish fossils relative to facies context, with bones collected from sandstones showing consistent enrichment in heavy REE. B) Bones recovered from continental sandstones and mudstones of the JRF show no significant distinctions in REE content in relation to facies context. C) The ecdfs of Pr_n content in fossils from sandstone facies (dashed) and mudstone facies (solid) of the TMF are distinct with a *p*-value of 2.1×10^{-5}. D) No significant distinctions were evident when REE content of fossil bone was compared among mudstone-hosted (solid) and sandstone-hosted (dashed) bonebeds of the JRF.

TMF, and JRF samples were collected <350 km to the south of DPF localities.

Cerium Anomalies in Upland versus Lowland Settings

Cerium anomalies in fossil bones have been used in previous studies of fossilization to infer redox conditions during early diagenesis, with the premise that negative anomalies indicate oxidizing conditions at the time of REE uptake (German and Elderfield, 1990; Dia et al., 2000). Positive Ce anomalies in fossil bone suggest diagenesis occurred under more reducing conditions or in the presence of saline alkaline-rich waters (German and Elderfield, 1990; Möeller and Bau, 1993; Martin et al., 2005). Metzger et al. (2004) documented both positive and negative anomalies in fossil bones recovered from the Oligocene Brule Formation of South Dakota, and attributed the positive anomalies to early diagenesis in reducing oxbow lake sediments. Suarez et al. (2007) also documented positive Ce anomalies in several dinosaur bones recovered from continental facies of the Crystal Geyser Quarry in the Lower Cretaceous Cedar Mountain Formation of Utah. The positive Ce anomaly was attributed to interaction with Ce-rich groundwaters interpreted to have evolved via the dissolution of manganese oxides (presumably pyrolusite) in underlying deposits of the Upper Jurassic Morrison Formation. Several other geochemical studies of fossil bone have reported predominantly negative Ce anomalies (e.g., Picard et al., 2002; Patrick et al., 2004; Labs-Hochstein and MacFadden, 2006; Tütken et al., 2008).

All but one of the fossil bones analyzed from the TMF and JRF exhibit negative Ce anomalies (Fig. 4), and this suggests that recrystallization in both units occurred in the presence of oxidizing pore waters. Fossil bones from the TMF are characterized by significantly more pronounced negative anomalies (−0.43 mean TMF versus −0.19 mean JRF), and this suggests that oxidation was more pervasive within the early diagenetic environments of the alluvial uplands. This reconstruction is consistent with the sedimentology of the upper TMF, which is characterized by red oxidized paleosols, abundant carbonate nodules ($CaCO_3$), and a relative dearth of macroscopic carbonaceous debris. Surficial sediments of the TMF alluvial plain were oxidizing and generally well drained. In contrast, the JRF is characterized by facies that show more indication of reduction in the form of abundant carbonaceous debris and siderite nodules. Nevertheless, all but one of the bones in the JRF sample yield negative Ce anomalies indicative of some degree of oxidation in early diagenetic environments. This presumably indicates the complexity of redox conditions in surficial deposits of the JRF coastal plain, which clearly encompassed both oxidizing and reducing microenvironments.

Uranium content in fossil bone has been shown to track the Ce anomaly in an inverse fashion, with more negative Ce values related to greater U concentrations (Metzger et al., 2004). This inverse correlation reflects the fact that U is more mobile in its oxidized state, and is apparently more readily incorporated into bones undergoing recrystallization in well-oxygenated settings. The pattern holds in this study, with U concentration correlating inversely with the Ce anomaly in both

TMF and JRF fossils (Fig. 4A). In JRF fossils U concentrations are relatively low, with only one bone exceeding 200 ppm. In the TMF sample six bones are characterized by U concentrations ranging from <280 to 690 ppm, and one bone has a U concentration of nearly 1000 ppm.

REE Patterns and Taphonomic History

Variations in ionic radius (the lanthanide contraction), pH and redox of postmortem environments, and site-specific hydrology, among other factors, generate fractionation patterns across the REE series that can be used to link recrystallized bones to specific diagenetic environments. These patterns have been used in previous studies of the REE to assess spatial mixing and time averaging in fossil assemblages, and to associate assemblages of fossils with particular depositional environments in both marine and continental settings (e.g., Trueman and Benton, 1997; Trueman, 1999; Patrick et al., 2004; Metzger et al., 2004; Martin et al., 2005; Anderson et al., 2007; Suarez et al., 2007). This information in turn can be used to advance and test taphonomic reconstructions.

With regard to assessing the potential for mixing, an assemblage of fossil bones that shows variable patterns of REE uptake arguably consists of fossils that recrystallized in different diagenetic environments prior to final accumulation and permanent burial. Alternatively, an assemblage of vertebrate fossils that exhibits variable REE content could have recrystallized through time in a locale where diagenetic conditions chemically evolved. None of the bonebeds examined in this study exhibit geochemical evidence indicative of significant spatial mixing. In contrast, all bonebeds sampled in the TMF and JRF show internally consistent patterns of REE uptake indicative of bones fossilizing in chemically stable depositional settings. Interestingly, other taphonomic and sedimentologic data indicate that the bonebeds in question may be time averaged over many successive generations (Rogers and Brady, 2010), but there is no indication that chemical conditions changed during the time frame of recrystallization.

The rare outliers in bonebed assemblages, such as the HREE-enriched bones in microfossil bonebeds TM-020 (Fig. 5B), UC-8303 (Fig. 5G), and UC-8439 (Fig. 5H) could be interpreted to represent inadvertent mixing of materials during collection, including the downslope addition of fossil remains from overlying fossiliferous units. Alternatively, seemingly anomalous REE patterns could indicate the complex distribution of REE in particular bioclasts. For example, LA-ICP-MS maps from bonebed UC-8303 (Koenig et al., 2009) reveal that trace element uptake can vary depending on the histology of individual bones. Maps of bones from UC-8303 exhibit concentration gradients dominated by light and middle REE at bone margins, and in one map (of the three generated) elevated concentrations of heavy REE are also developed in the bone core. Koenig et al. (2009) interpreted this to reflect preferential capture of light and middle REE via the diffusion-adsorption mechanism at outer edges of bones and subsequent movement of waters enriched in heavy REE within inner vascular networks. In bones that show such complexity, distinctly different fractionation patterns can result from mm-scale deviations in the targeting of a laser or drill bit.

With regard to tracking REE content in relation to particular facies, Trueman (1999) proposed a general model for alluvial records that compares geochemical signatures of bones that recrystallize in soils with bones that recrystallize in stream channels. In his model, the heavy REE form stable aqueous complexes with ligands (organic, carbonate, phosphate) in weathering profiles of soils, and remain in solution, ultimately migrating with pore waters to channel belts, where they concentrate and come in contact with recrystallizing bones. In contrast, the light REE are preferentially adsorped onto mineral surfaces and bound to organic particles in the weathering profile, and remain in soils. If light REE are subsequently released into solution they will be preferentially incorporated into bones undergoing recrystallization. In summary, this model predicts that bones that undergo recrystallization in well-drained soils will be relatively enriched in light REE, whereas bones that undergo recrystallization in rivers and streams will be relatively enriched in heavy REE. Trueman (1999) tested this model in fossils recovered from the TMF near Choteau, Montana, and found general agreement, with bones derived from fine-grained overbank deposits enriched in light REE and bones derived from sandstones enriched in heavy REE. Readers should consult Metzger et al. (2004), Martin et al. (2005), and Suarez et al. (2007) for additional considerations of REE patterning in continental systems.

Lithology-related patterns in the fractionation of the REE are also apparent in the TMF fossils analyzed in this study (Figs. 5–6). Bones that recrystallized in pond-lake microfossil bonebeds in floodplain deposits are relatively enriched in middle REE, whereas isolated bones recovered from sandstone bodies are enriched in heavy REE. This pattern of REE content is consistent with the model of Trueman (1999) described earlier, at least in relation to the relative enrichment of heavy REE in bones collected from channel deposits. The absence of light REE enrichment in bones recovered from floodplain deposits of the TMF likely indicates that the depositional environments sampled for fossil bone were not well-drained weathering profiles where light REE would be expected to accumulate, but rather poorly drained subaqueous settings where the translocation of complexed REE would be impeded.

Lithology-based distinctions in REE content are not developed in the JRF (Figs. 5–6), where both pond-lake microfossil bonebeds and channel-hosted microfossil bonebeds are characterized by relative depletion of light REE, coupled with minor enrichment of middle REE and, to a somewhat lesser extent, heavy REE. The generally similar patterns of REE content that characterize assemblages of fossils recovered from channel-hosted and floodplain-hosted (pond-lake) bonebeds in the JRF are interpreted to reflect at least two factors. First, three of the JRF bonebeds under investigation (UC-8302A, UC-8303, UC-914) formed in ancient floodbasin ponds-lakes on the Judith River coastal plain (Rogers and Brady, 2010). Bones recovered from these three sites presumably recrystallized in comparable sedimentary facies (carbonaceous mudstones), and would be expected to have similar REE content.

The second potential explanation for similar REE content in bones recovered from floodplain-hosted and channel-hosted bonebeds of the JRF relates to the origin of the fossil assemblages that comprise channel-hosted sites. In a recent consideration of the formative processes that generate microfossil bonebeds in the JRF (Rogers and Brady, 2010), various lines of geologic and taphonomic evidence were brought to bear on the question of how localized concentrations of vertebrate microfossils potentially accumulated in fluvial channels. Data indicate that vertebrate hardparts initially accumulated to fossiliferous levels via attritional processes in ponds-lakes on the JRF coastal plain and were subsequently reworked and redeposited as channel-hosted assemblages in close proximity to source beds. This reconstruction is grounded in reasonable expectations of lacustrine and fluvial depositional systems and is consistent with faunal data that indicate that channel-hosted assemblages and pond-lake assemblages in the JRF are similar with regard to the presence/absence and rank order abundance of taxa. This taphonomic reconstruction is counter to the commonly held view that microfossil bonebeds preserved in channel deposits are biased samples that have experienced long-distance transport and significant hydrodynamic sorting.

Geochemical data can be used to test this taphonomic reconstruction in the JRF record. The bone assemblage in bonebed UC-8302 is localized in the lower 30 cm of a 7-m-thick, fine-grained sandstone body (Figs. 7A–C). Vertebrate fossils are preserved in association with abundant "*Unio*" debris, fragmentary shells of smaller freshwater invertebrates (*Sphaerium* and *Viviparus*), ironstone and claystone

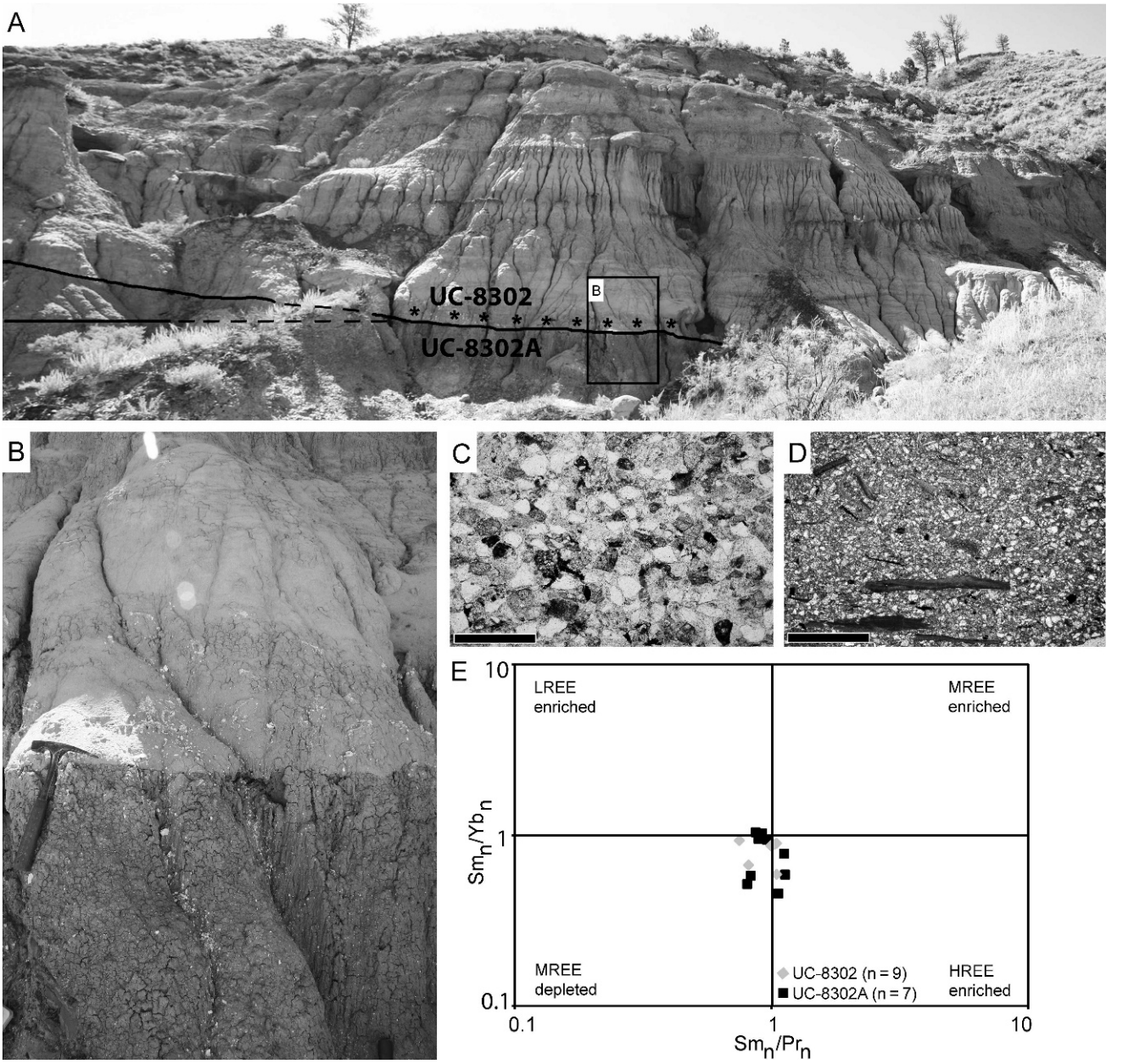

FIGURE 7—Field view of JRF bonebeds UC-8302 and UC-8302A. A) The sandstone body hosting UC-8302 cuts down through several meters of interchannel deposits, including the full thickness of bed B, and in its most fossiliferous expanse (indicated by asterisks) intersects pond-lake microfossil bonebed UC-8302A. The sandstone body hosting UC-8302 continues downcutting to the right; contact obscured by vegetated slope in foreground. B) Close-up view of contact between bonebed UC-8302 and bonebed UC-8302A. C) Photomicrograph of sandstone matrix of bonebed UC-8302 (scale bar 1 mm). D) Photomicrograph of clay-rich siltstone matrix of bonebed UC-8302A (scale bar 1 mm). E) Box plot comparing REE content of fossils from both bonebeds.

pebbles, and coaly stringers. The sandstone body hosting UC-8302 erodes down through several meters of fine-grained interchannel deposits, and in its most fossiliferous expanse intersects bonebed UC-8302A. UC-8302A is a 45 cm thick pond-lake bonebed that preserves dispersed vertebrate fossils in a massive clay-rich siltstone matrix that also yields abundant laminated carbonaceous debris and the shells and shell fragments of *Sphaerium*, *Viviparus*, and other small freshwater invertebrates (Figs. 7B, D). Geochemical data from these two localities indicate that they are indistinguishable from a diagenetic perspective, at least in relation to the uptake of REE (Figs. 5E–F, 7E). This, in turn, is consistent with vertebrate fossils in UC-8302 and UC-8302A sharing the same early taphonomic history, with all bones initially recrystallizing in the fine-grained facies of UC-8302A. After REE had been incorporated and essentially locked into bone tissue, a subset of the fossilized material in UC-8302A was reworked and incorporated into sandstone deposits of UC-8302. It is important to note, however, that the small sample sizes used to make statistical comparisons yield low power to detect differences between the two localities. Nevertheless, geochemical data are consistent with the reworking and redeposition of a preexisting concentration of recrystallized fossil bones in the JRF.

SUMMARY AND CONCLUSIONS

In this study, REE content of a large sample of fossil bone of Late Cretaceous age was determined using LA-ICP-MS. Multiple line scans were targeted across compact bone tissue in each element (n = 76), and these were individually integrated and then averaged to determine REE content on a per bone basis. With detection limits for the REE of ~0.1–

0.5 ppm, LA-ICP-MS is well suited for studies of diagenesis in fossilized bioapatite, and is an ideal analytical approach when abundant samples need to be processed.

Samples from seven microfossil bonebeds and several additional isolated elements from the TMF and JRF of Montana were analyzed using LA-ICP-MS, and results show general consistency with previous work in these same two units based on standard ICP-MS techniques (Trueman, 1999). Fossils are differentiable at the formation scale, with samples in the TMF characterized by generally higher overall REE content, and more variability in REE enrichment, than counterparts in the JRF. Statistically distinct patterns in the distribution of specific REE also serve to distinguish fossils recovered from the two formations. Bones in the JRF are relatively enriched in heavy REE, whereas bones analyzed from the TMF span heavy and light enrichment fields in approximately equal proportions. Fossil bones from the TMF are also characterized by significantly more negative Ce anomalies (and greater U enrichment) than counterparts in the JRF record, and this presumably reflects the more oxidizing upland setting of fossilization for the TMF sample.

REE data also show general consistency within the bonebeds under investigation, and there is no geochemical indication of spatial or temporal mixing. There is good indication, however, that many of the bonebeds in question are in fact attritional assemblages that accumulated over considerable time spans (10^2–10^3 yrs) in localized aquatic basins (Rogers and Brady, 2010). Accordingly, the absence of evidence for geochemical mixing in a fossil assemblage must be evaluated carefully, and compared with other independent indicators of taphonomic history, such as sedimentological context and the preservational quality of bioclasts (see for example Anderson et al., 2007; Suarez et al., 2007). In the case of the TMF and JRF pond-lake microfossil bonebeds, bioclasts apparently recrystallized in long-lived aquatic settings that remained chemically and hydrologically stable. The time-averaged nature of these assemblages is not revealed by their REE geochemistry.

Finally, lithology-related distinctions in REE content were documented, and some expected patterns emerged. For example, isolated fossil bones recovered from sandstone deposits of the TMF were relatively enriched in heavy REE as models predict (e.g., Trueman, 1999). In contrast, bonebed samples analyzed from the JRF, regardless of facies context, exhibited similar patterns of REE uptake. This finding is consistent with ongoing taphonomic work in the JRF that suggests that channel-hosted microfossil bonebeds are reworked subsamples of preexisting concentrations that accumulated in floodbasin ponds and lakes (Rogers and Brady, 2010). The current study provides important geochemical insights that further suggest that reworked elements, at least in some cases, were delivered to channels in a prefossilized condition (see also Rogers and Kidwell, 2000). This reconstruction, if correct (and additional analyses are planned), provides insights into the timing of early diagenesis, and indicates that REE were already incorporated into bones in near-surface sediments prior to their being reworked and re-deposited by active Cretaceous channels traversing the Judith River coastal plain.

ACKNOWLEDGMENTS

Financial support was provided by National Science Foundation EAR-0319041, National Science Foundation EAR-0319024, the Beltmann Research Fund (Macalester College), and the Minnesota Space Grant Consortium (Macalester College). We thank two anonymous reviewers for suggestions that improved the manuscript. We also thank C. N. Trueman for insights related to rare earth elements and bone diagenesis, and J. H. Hartman, who identified mollusks recovered from Judith River bonebeds. The Bureau of Land Management is acknowledged for providing permits and logistical support in the Upper Missouri River Breaks National Monument. Finally, we thank Ricky Reagan of Browning, Montana, who graciously provided access to the rocks at Landslide Butte.

REFERENCES

Anderson, P.E., Benton, M.J., Trueman, C.N., Paterson, B.A., and Cuny, G., 2007, Palaeoenvironments of vertebrates on the southern shore of Tethys: The nonmarine Early Cretaceous of Tunisia: Palaeogeography, Palaeoclimatology, Palaeoecology, v. 243, p. 118–131.

Barker, M.J., Clarke, J.B., and Martill, D.M., 1997, Mesozoic reptile bones as diagenetic windows: Bulletin de la Société Géologique de France, v. 168, p. 535–545.

Brophy, G.P., and Nash, J.T., 1968, Compositional, infrared, and x-ray analysis of fossil bone: The American Mineralogist, v. 53, p. 445–454.

Clementz, M.T., Holroyd, P.A., and Koch, P.L., 2008, Identifying aquatic habits of herbivorous mammals through stable isotope analysis: PALAIOS, v. 23, p. 574–585.

Dia, A., Gruau, G., Olivie-Lauquet, G., Riou, C., Molenat, J., and Curmi, P., 2000, The distribution of rare earth elements in groundwaters: Assessing the role of source-rock composition, redox changes and colloidal particles: Geochimica et Cosmochimica Acta, v. 64, p. 4131–4151.

Durrant, S.F., 1999, Laser ablation inductively coupled plasma mass spectrometry: Achievements, problems, prospects: Journal of Analytical Atomic Spectrometry, v. 14, 1385–1403.

Durrant, S.F., and Ward, N.I., 2005, Recent biological and environmental applications of laser ablation inductively coupled plasma mass spectrometry (LA-ICP-MS): Journal of Analytical Atomic Spectrometry, v. 20, p. 821–829.

Eberth, D.A., Shannon, M., and Noland, B.G., 2007, A bonebeds database: Classification, biases and patterns of occurrence, *in* Rogers, R.R., Eberth, D.A., and Fiorillo, A.R., eds., Bonebeds: Genesis, Analysis, and Paleobiological Significance: University of Chicago Press, Chicago, p. 103–219.

Eggins, S., De Deckker, P., and Marshall, J., 2003, Mg/Ca variation in planktonic foraminifera tests: Implications for reconstructing palaeo-seawater temperature and habitat migration: Earth and Planetary Science Letters, v. 212, p. 291–306.

Elorza, J., Astibia, H., Murelaga, X., and Pereda-Superbiola, X., 1999, Francolite as a diagenetic mineral in dinosaur and other Upper Cretaceous reptile bones (Laño, Iberian Peninsula): microstructural, petrological and geochemical features: Cretaceous Research, v. 20, p. 169–187, doi: 10.1006/cres.1999.0144.

Falcon-Lang, H.J., 2003, Growth interruptions in conifer woods from the Upper Cretaceous (Campanian) Two Medicine Formation, Montana, USA: Implications for palaeoclimate and dinosaur ecology: Palaeogeography, Palaeoclimatology, Palaeoecology, v. 199, p. 299–331.

Foreman, B.Z., Rogers, R.R., Deino, A.L., Wirth, K.R., and Thole, J.T., 2008, Geochemical characterization of bentonite beds in the Two Medicine Formation (Campanian, Montana), including a new $^{40}Ar/^{39}Ar$ age: Cretaceous Research, v. 29, p. 373–385.

Fricke, H.C., and Rogers, R.R., 2000, Multiple taxon-multiple locality approach to providing oxygen isotope evidence for warm-blooded theropod dinosaurs: Geology, v. 28, p. 799–802.

Fricke, H.C., Rogers, R.R., and Gates, T.A., 2009, Hadrosaurid migration: inferences based on stable isotope comparisons among Late Cretaceous dinosaur localities: Paleobiology, v. 35, p. 270–288.

German, C.R., and Elderfield, H., 1990, Application of the Ce anomaly as a paleoredox indicator: The ground rules: Paleoceanography, v. 5, p. 823–833.

Goodwin, M.B., and Deino, A.L., 1989, The first radiometric ages from the Judith River Formation (Late Cretaceous), Hill County, Montana: Canadian Journal of Earth Sciences, v. 26, p. 1384–1391.

Google, 2007, Google Earth, http://earth.google.com.

Gromet, L.P., Dymek, R.F., Haskin, L.A., and Korotev, R.L., 1984, The "North American shale composite": Its compilation, major and trace element characteristics: Geochimica et Cosmochimica Acta, v. 48, p. 2469–2482.

Grün, R., Aubert, M., Joannes-Boyau, R., and Moncel, M-H., 2008, High resolution analysis of uranium and thorium concentration as well as U-series isotope distributions in a Neanderthal tooth from Payre (Ardèche, France) using laser ablation ICP-MS: Geochimica Cosmochimica Acta, v. 72, p. 5278–5290.

Haskin, L.A., Haskin, M.A., Frey, F.A., and Wildeman, T.R., 1968, Relative and absolute terrestrial abundances of the rare earths, *in* Ahrens, L.H., ed., Origin and Distribution of the Elements: Pergamon, Oxford, p. 889–912.

Hubert, J.F., Panish, P.T., Chure, D.J., and Prostak, K.S., 1996, Chemistry, microstructure, petrology and diagenetic model of Jurassic dinosaur bones, Dinosaur National Monument, Utah: Journal of Sedimentary Research, v. 66, p. 531–547.

Imai, N., 1992, Microprobe analysis of geological materials by laser ablation inductively coupled plasma mass spectrometry: Analytica Chimica Acta, v. 269, p. 263–268.

KOENIG, A.E., ROGERS, R.R., and TRUEMAN, C.N., 2009, Visualizing fossilization using laser-ablation inductively coupled plasma-mass spectrometry maps of trace elements in Late Cretaceous bones: Geology, v. 37, p. 511–514.

KOHN, M.J., 2008, Models of diffusion-limited uptake of trace elements in fossils and rates of fossilization: diagenetic mechanisms and the role of sediment pore fluids: Geochimica et Cosmochimica Acta, v. 72, p. 3758–3770.

KOLODNY, Y., BOAZ, L., SANDER, M., and CLEMENS, W.A., 1996, Dinosaur bones; fossils or pseudomorphs? The pitfalls of physiology reconstruction from apatitic fossils: Palaeogeography, Palaeoclimatology, Palaeoecology, v. 126, p. 161–171.

LABS-HOCHSTEIN, J., and MACFADDEN, B.J., 2006, Quantification of diagenesis in Cenozoic sharks: Elemental and mineralogical changes: Geochimica et Cosmochimica Acta, v. 70, p. 4921–4932.

LONGERICH, H., JACKSON, S., and GUNTHER, D., 1996, Laser ablation inductively coupled plasma mass spectrometric transient signal data acquisition and analyte concentration calculation: Journal of Analytical Atomic Spectrometry, v. 22, p. 899–904.

LORENZ, J.C., 1981, Sedimentary and tectonic history of the Two Medicine Formation, Late Cretaceous (Campanian), northwestern Montana: Unpublished Ph.D. thesis, Princeton University, Princeton, New Jersey, 215 p.

MACFADDEN, B.J., LABS-HOCHSTEIN, J., QUITMYER, I., and JONES, D.S., 2004, Incremental growth and diagenesis of skeletal parts of the lamnoid shark *Otodus obliquus* from the early Eocene (Ypresian) of Morocco: Palaeogeography, Palaeoclimatology, Palaeoecology, v. 206, p. 179–192.

MACFADDEN, B.J., SOLOUNIAS, N., and CERLING, T.E., 1999, Ancient diets, ecology, and extinction of 5-million-year-old horses from Florida: Science, v. 283, p. 824–827.

MARTIN, J.E., PATRICK, D., KIHM, A.J., FRANKLIN, F.F., and GRANDSTAFF, D.E., 2005, Lithostratigraphy, tephrochronology, and rare earth element geochemistry of fossils at the Classical Pleistocene Fossil Lake area, south central Oregon: Journal of Geology, v. 113, p. 139–156.

METZGER, C.A., TERRY, D.O., and GRANDSTAFF, D.E., 2004, Effect of paleosol formation on rare earth element signatures in fossil bone: Geology, v. 32, p. 497–500.

MÖELLER, P., and BAU, M., 1993, Rare-earth patterns with positive cerium anomaly in alkaline waters from Lake Van, Turkey: Earth and Planetary Science Letters, v. 117, p. 671–676.

OGG, J.G., OGG, G., and GRADSTEIN, F.M., 2008, The Concise Geologic Time Scale: Cambridge University Press, Cambridge, 177 p.

PATRICK, D., MARTIN, J.E., PARRIS, J.E., and GRANDSTAFF, G.E., 2004, Paleoenvironmental interpretations of rare earth element signatures in mosasaurs (reptilia) from the upper Cretaceous Pierre Shale, central South Dakota, USA: Palaeogeography, Palaeoclimatology, Palaeoecology, v. 212, p. 277–294.

PERSON, A., BOCHERENS, H., SALIÈGE, J.-F., PARIS, F., ZEITOUN, V., and GÉRARD, M., 1995, Early diagenetic evolution of bone phosphate: An x-ray diffractometry analysis: Journal of Archaeological Science, v. 22, p. 211–221.

PICARD, S., LÉCUYER, C., BARRAT, J.-A., PIERRE, J.-P., DROMART, G., and SHEPPARD, S.M.F., 2002, Rare earth element contents of Jurassic fish and reptile teeth and their potential relation to seawater composition (Anglo-Paris Basin, France and England): Chemical Geology, v. 186, p. 1–16.

PIEPENBRINK, H., 1989, Examples of chemical changes during fossilization: Applied Geochemistry, v. 4, p. 273–280.

REYNARD, B., LÉCUYER, C., and GRANDJEAN, P., 1999, Crystal-chemical controls on rare earth element concentrations in fossil biogenic apatites and implications for paleoenvironmental reconstructions: Chemical Geology, v. 155, p. 233–241.

RODLAND, D.L., KOWALEWSKI, M., DETTMAN, D.L., and FLESSA, K.W., 2003, High-resolution analysis of $\delta^{18}O$ in the biogenic phosphate of modern and fossil lingulid brachiopods: Journal of Geology, v. 111, p. 441–453.

ROGERS, A.F., 1924, Mineralogy and petrography of fossil bone: Geological Society of America Bulletin, v. 35, p. 535–556.

ROGERS, R.R., 1990, Taphonomy of three dinosaur bone beds in the Upper Cretaceous Two Medicine Formation, northwestern Montana: Evidence for drought-related mortality: PALAIOS, v. 5, p. 394–413.

ROGERS, R. R., 1993, Systematic patterns of time averaging in the terrestrial vertebrate record: A Cretaceous case study, *in* Kidwell, S.M., and Behrensmeyer, A.K., eds., Taphonomic Approaches to Time Resolution in Fossil Assemblages, Short Courses in Paleontology 6, Paleontological Society, Knoxville, Tennessee, p. 228–249.

ROGERS, R.R., 1994, Nature and origin of through-going discontinuities in nonmarine foreland basin deposits, Upper Cretaceous, Montana: Implications for sequence analysis: Geology, v. 22, p. 1119–1122.

ROGERS, R.R., 1995, Sequence stratigraphy and vertebrate taphonomy of the Upper Cretaceous Two Medicine and Judith River formations, Montana: Unpublished Ph.D. thesis, University of Chicago, Chicago, 400 p.

ROGERS, R.R., 1998, Sequence analysis of the upper Cretaceous Two Medicine and Judith River formations, Montana: Nonmarine response to the Claggett and Bearpaw marine cycles: Journal of Sedimentary Research, v. 68, p. 615–631.

ROGERS, R.R., and BRADY, M.E., 2010. Origins of microfossil bonebeds: Insights from the Upper Cretaceous Judith River Formation of north-central Montana. Paleobiology, v. 36, p. 80–112.

ROGERS, R.R., and KIDWELL, S.M., 2000, Associations of vertebrate skeletal concentrations and discontinuity surfaces in terrestrial and shallow marine records: A test in the Cretaceous of Montana: Journal of Geology, v. 108, p. 131–154.

ROGERS, R.R., and KIDWELL, S.M., 2007, A conceptual framework for the genesis and analysis of vertebrate skeletal concentrations, *in* Rogers, R.R., Eberth, D.A., and Fiorillo, A.R., eds., Bonebeds: Genesis, Analysis, and Paleobiological Significance: University of Chicago Press, Chicago, p. 1–63.

ROGERS, R.R., and SWISHER, C.C., 1996, The Claggett and Bearpaw transgressions revisited; new $^{40}Ar/^{39}Ar$ data and a review of possible drivers: Abstracts with Programs, Geological Society of America, v. 28(6), p. 62.

ROGERS, R.R., SWISHER, C.C., and HORNER, J.R., 1993, $^{40}Ar/^{39}Ar$ age and correlation of the non-marine Two Medicine Formation (Upper Cretaceous), northwestern Montana: Canadian Journal of Earth Sciences, v. 30, p. 1066–1075.

SAMOILOV, D.L., and BENJAMINI, C., 1996, Geochemical features of dinosaur remains from the Gobi Desert, South Mongolia: PALAIOS, v. 11, p. 519–531.

SCHWEIZER, M.K., STEELE, A., TOPORSKI, J.K.W., and FOGEL, M.L., 2007, Stable isotopic evidence for fossil food webs in Eocene Lake Messel: Paleobiology, v. 33, p. 590–609.

SHEMESH, A., 1990, Crystallinity and diagenesis of sedimentary apatites: Geochimica et Cosmochimica Acta, v. 54, p. 2433–2438.

SPONHEIMER, M., and LEE-THORP, J., 1999, Alteration of enamel carbonate environments during fossilization: Journal of Archaeological Science, v. 26, p. 143–150.

STARON, R.M., GRANDSTAFF, B.S., GALLAGHER, W.B., and GRANDSTAFF, D.E., 2001, REE signatures in vertebrate fossils from Sewell, NJ: Implications for location of the K-T boundary: PALAIOS, v. 16, p. 255–265.

SUAREZ, C.A., SUAREZ, M.B., TERRY, D.O., and GRANDSTAFF, D.E., 2007, Rare earth element geochemistry and taphonomy of the Early Cretaceous Crystal Geyser dinosaur quarry, east-central Utah: PALAIOS, v. 22, p. 500–512.

TOOTS, H., 1963, The chemistry of fossil bones from Wyoming and adjacent states: Contributions to Geology, University of Wyoming, v. 2, p. 69–80.

TRUEMAN, C.N., 1999, Rare earth element geochemistry and taphonomy of terrestrial vertebrate assemblages: PALAIOS, v. 14, p. 555–568.

TRUEMAN, C.N., 2007, Trace element geochemistry of bonebeds, *in* Rogers, R.R., Eberth, D.A., and Fiorillo, A.R., eds., Bonebeds: Genesis, Analysis and Paleobiological Significance: University of Chicago Press, Chicago, p. 397–435.

TRUEMAN, C.N., BEHRENSMEYER, A.K., POTTS, R., and TUROSS, N., 2006, High-resolution records of location and stratigraphic provenance from rare earth element composition of fossil bone: Geochimica et Cosmochimica Acta, v. 70, p. 4343–4355.

TRUEMAN, C.N., BEHRENSMEYER, A.K., TUROSS, N., and WEINER, S., 2004, Mineralogical and compositional changes in bones exposed on soil surfaces in Amboseli National Park, Kenya: diagenetic mechanisms and the role of sediment pore fluids: Journal of Archeological Science, v. 31, p. 721–739.

TRUEMAN, C.N., and BENTON, M.J., 1997, A geochemical method to trace the taphonomic history of reworked bones in sedimentary settings: Geology, v. 25, p. 263–266.

TRUEMAN, C.N., BENTON, M.J., and PALMER, M.R., 2003, Geochemical taphonomy of shallow marine assemblages: Palaeogeography, Palaeoclimatology, Palaeoecology, v. 197, p. 151–169.

TRUEMAN, C.N., PALMER, M.R., FIELD, J., PRIVAT, K., LUDGATE, N., CHAVAGNAC, V., EBERTH, D.A., CIFELLI, R., and ROGERS, R.R., 2008, Comparing rates of recrystallisation and the potential for preservation of biomolecules from the distribution of trace elements in fossil bones: Palevol, v. 7, p. 145–158.

TRUEMAN, C.N., and TUROSS, N., 2002, Trace elements in recent and fossil bone apatite, *in* Kohn, M.J., Rakovan, J., and Hughes, J.M., eds., Phosphates: Geochemical, Geobiological, and Materials Importance, Reviews in Mineralogy and Geochemistry, v. 48, p. 489–521.

TÜTKEN, T., VENNEMANN, T.W., and PFRETZSCHNER, H.-U., 2008, Early diagenesis of bone and tooth apatite in fluvial and marine settings: Constraints from combined oxygen isotope, nitrogen and REE analysis: Palaeogeography, Palaeoclimatology, Palaeoecology, v. 266, p. 254–268.

WEINER, S., and BAR-YOSEF, O., 1990, States of preservation of bones from prehistoric sites in the near east: A survey: Journal of Archaeological Science, v. 17, p. 187–196.

WINGS, O., 2004, Authigenic minerals in fossil bones from the Mesozoic of England: poor correlation with depositional environments: Palaeogeography, Palaeoclimatology, Palaeoecology, v. 214, p. 15–32.

WRIGHT, J., SCHRADER, H., and HOLSER, WT., 1987, Paleoredox variations in ancient oceans recorded by rare earth elements in fossil apatite: Geochimica et Cosmochimica Acta, v. 51, p. 631–644.

ACCEPTED NOVEMBER 26, 2009